Oil–Water Separation

International Edition: DOI: 10.1002/anie.201507692
German Edition: DOI: 10.1002/ange.201507692

Biomimetic Superhydrophobic/Superoleophilic Highly Fluorinated Graphene Oxide and ZIF-8 Composites for Oil–Water Separation

Kolleboyina Jayaramulu[+], Kasibhatta Kumara Ramanatha Datta[+], Christoph Rösler, Martin Petr, Michal Otyepka, Radek Zboril, and Roland A. Fischer**

Abstract: *Superhydrophobic/superoleophilic composites* ***HFGO@ZIF-8*** *have been prepared from highly fluorinated graphene oxide (HFGO) and the nanocrystalline zeolite imidazole framework ZIF-8. The structure-directing and coordination-modulating properties of HFGO allow for the selective nucleation of ZIF-8 nanoparticles at the graphene surface oxygen functionalities. This results in localized nucleation and size-controlled ZIF-8 nanocrystals intercalated in between HFGO layers. The composite microstructure features fluoride groups bonded at the graphene. Self-assembly of a unique micro-mesoporous architecture is achieved, where the micropores originate from ZIF-8 nanocrystals, while the functionalized mesopores arise from randomly organized HFGO layers separated by ZIF-8 nanopillars. The hybrid material displays an exceptional high water contact angle of 162° and low oil contact angle of 0° and thus reveals very high sorption selectivity, fast kinetics, and good absorbencies for nonpolar/polar organic solvents and oils from water. Accordingly,* ***Sponge@HFGO@ZIF-8*** *composites are successfully utilized for oil–water separation.*

Oil spills in oceans and rivers are a serious danger to marine species and human beings, leading to a long-term threat to public health and the environment.[1,2] The separation of oil from water without causing environmental pollution is a challenging task. The traditional oil-spill cleaning technologies include separation, filtration, centrifugation, floatation, and electrochemical methods.[2] Among the various methods developed for the removal of oil from water, separation holds great promise due to its simplicity, high efficiency, and relatively low cost.[3] Nature-inspired superhydrophobic materials (lotus leaf, butterfly wings) have gained much importance for application in oil-spill cleaning.[4]

It has been realized that not only superhydrophobicity (a water contact angle more than 150°) but also superoleophillicity (an oil contact angle of less than 10°) is crucial for efficient oil absorption in the presence of water.[5] Traditional materials of this kind can be obtained that have features like rough structure on a waxy surface with low surface energy.[6] Design concepts include polymer sponges, porous graphitic carbon and its composites, polymethylsilsesquioxane aerogels, membranes with nanowires, and steel meshes and fabrics (Table S1 in the Supporting Information).[6–8] However fabricating such materials can be demanding and may have limitations in terms of practical applications because of expensive components and time-consuming and multistep procedures. The development of superior superhydrophobic/superoleophilic materials still represents a major challenge. Facile, cheap, and scalable synthesis is desirable and a number of key properties need to be integrated in one material such as low density, large internal surface area with hierarchical pore structure, low water uptake, and excellent reusability.

Recently, porous crystalline coordination polymers, also called metal–organic frameworks (MOFs), in which a hybrid array of inorganic metal ions chelated with various organic linkers yields ordered pores with exceptional high internal surface area, have become subjects of tremendous interest across many disciplines.[9] A number of very hydrophobic MOFs based on (long-chain) alkyl substituents[10a] and/or fluorine-containing linkers[10b–e] are known. Their adaptable hydrophobic surfaces inhibit the penetration of water molecules into pores. The early report by M. E. Omary on this kind of fluorinated MOFs for oil–water separation is highlighted here.[10d] An idea going beyond the limitations of existing concepts of tailoring the functional properties of MOFs based on node/linker combination, topology, and linker design would be the hybridization of MOFs with other suitable components, such as graphene and its derivatives.[11] In particular, fluorographene has recently received attention due to its remarkable optical, chemical, and biological properties.[12] The decoration of oxygen functionalities over highly fluorinated graphene oxide (HFGO) offers scope for diverse chemical functionalization and loading capabilities. Herein we report a new strategy to prepare functional porous hybrids comprising HFGO and zeolite imidazole frameworks (ZIFs) through a bottom-up solution-assisted self-assembly route.

Zeolite imidazole frameworks (ZIFs) are very robust porous coordination polymers (MOFs) exhibiting exceptional chemical stability and flexibility, and used in attractive applications in catalysis and in gas storage and separation.[13–15] We selected ZIF-8 for hybridization with HFGO because of its cheap and easy preparation and its well-established nano-/mesoscale surface chemistry at various substrates.[14] The in situ formed ZIF-8 nanocrystals act as

[*] Dr. K. Jayaramulu,[+] C. Rösler, Prof. Dr. R. A. Fischer
Inorganic Chemistry II-Organometallics and Materials Chemistry
Ruhr University Bochum, 44870 Bochum (Germany)
E-mail: roland.fischer@rub.de
Dr. K. K. R. Datta,[+] M. Petr, Prof. Dr. M. Otyepka, Prof. Dr. R. Zboril
Regional Centre of Advanced Technologies and Materials
Department of Physical Chemistry
Faculty of Science, Palacky University
Šlechtitelů 27, 78371 Olomouc (Czech Republic)
E-mail: radek.zboril@upol.cz
[+] These authors contributed equally to this work.

Supporting information for this article is available on the WWW under http://dx.doi.org/10.1002/anie.201507692.

pillars that intercalate between fluorinated graphene oxide layers through selective nucleation and controlled growth during liquid-phase nano-ZIF-8 synthesis (Scheme 1 and Scheme S1 in the Supporting Information). The implementation of ZIF-8 nanopillars between the HFGO layers provides the hybrid with additional mesoporosity. The low surface energy of the polar C–F bonds at the graphene surface considerably affects the wetting properties of the resultant **HFGO@ZIF-8** hybrid and endows it with excellent superhydrophobic along with superoleophilic behavior. The intrinsically hydrophobic ZIF-8 with its microscale roughness and also the chemical composition of the HFGO surface contribute to this synergy.

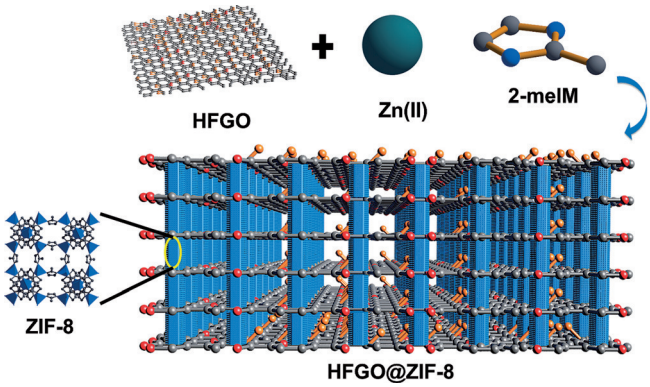

Scheme 1. Illustration showing the concept of the formation and structure of **HFGO@ZIF-8** (see also Scheme S1 in the Supporting Information). ZIF-8: $Zn(meIM)_2$, meIM = 2-methylimidazole, HFGO = highly fluorinated graphene oxide.

Accordingly, **HFGO@ZIF-8** was tested for the separation of organic solvents and oils from water with high selectivity, good recyclability, and fast absorption kinetics and a new material **Sponge@HFGO@ZIF-8** was exploited for the effective separation of oil (petroleum) from water. The **HFGO@ZIF-8** hybrid samples were prepared by the addition of a mixture of exfoliated HFGO sheets in chloroform during the formation of ZIF-8 nanocrystals at the liquid–solid interface in methanolic medium (see Experimental Section in the Supporting Information). Few-layered HFGO sheets are obtained by sonicating HFGO in chloroform for one hour. These exfoliated sheets provide the host substrate for the surface nucleation and growth of ZIF-8 nanocrystals. The powder X-ray diffraction pattern of the resultant hybrid shows all major crystallographic planes that can be indexed to pristine ZIF-8 (Figure 1). The interfacial contact of ZIF-8 nanocrystals with HFGO is difficult to unambiguously establish by X-ray diffraction data (see Figure S2 in the Supporting Information).[11a]

The X-ray photoelectron spectrum (XPS) of HFGO shows signals from the elements carbon, fluorine, and oxygen (detailed structural and bonding information is provided in Supporting Information, Figure S4). The C/F/O atomic ratio in HFGO was found to be 1:0.78:0.17. The high-resolution C 1s and F 1s core-level spectra of HFGO provide more information on the C–F bonding, as shown in Figure S4.

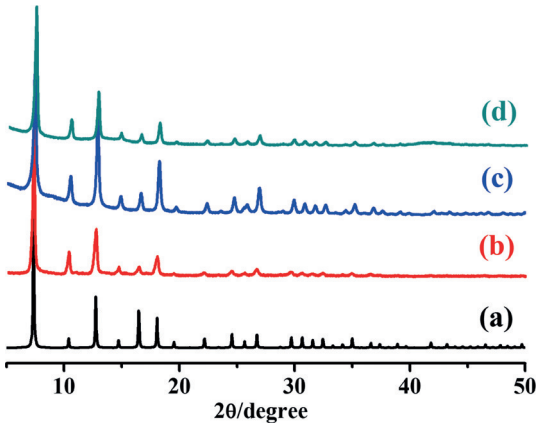

Figure 1. Powder XRD patterns of a) simulated ZIF-8; b) as-synthesized ZIF-8; c) **HFGO@ZIF-8** composite; d) activated **HFGO@ZIF-8** composite at 160 °C.

The structure consists almost entirely of covalent C–F bonding, with minor contributions from $C–F_2$, C–O, C=O, C–F (ionic), and C=C bonding. The O 1s spectrum shows the bonding associated with C–O, and C=O bonding with minimal contribution coming from O–F bonding.

For the **HFGO@ZIF-8** composite we observe the elements Zn and N in addition to the C, F, and O components (Figure S5). The characteristic Zn peaks at binding energies 1021.6 and 1045.6 eV were observed corresponding to Zn 2p3/2 and Zn 2p1/2, respectively. N 1s spectrum shows a peak related to imine which corresponds to the imidazole functional entity at 398.7 eV. Importantly the chemical nature of the fluorine groups (covalent C–F bonds) of **HFGO@ZIF-8** were not altered during the synthesis process. These crystallographic and spectroscopic data support the structural model of successive HFGO layers and the coordination of exposed Zn^{2+} cations to oxygen functionalities of HFGO (Figure S3).

The morphologies of HFGO, ZIF-8, and **HFGO@ZIF-8** were evaluated by using various microscopic techniques (Figure 2). The low-contrast (transparent) sheet-like form of HFGO is clearly evident from the transmission electron microscopy (TEM) image, with a few sheets being twisted (Figure 2a). The TEM micrograph of ZIF-8 shows nanocrystals with hexagonal morphology and sizes ranging from 70 to 160 nm. Importantly, the ZIF-8 nanocrystals are very well dispersed and intercalated between HFGO layers (see HRTEM image in Figure 2c, HAADF-STEM images in Figure 2d and Figure S6, and AFM image in Figure S7). Based on these observations it is concluded that HFGO acts as a functional support (structure-directing) as well as a coordination-modulating agent for nanoscale ZIF-8 growth.

Nitrogen adsorption–desorption isotherms obtained at 77 K proved that the ZIF-8 component exhibits the expected type-I isotherm characteristic of microporous materials with a specific surface area of 1150 $m^2 g^{-1}$ (Figure S8a). Pristine HFGO, on the other hand, exhibits a type-II isotherm characteristic for nonporous materials with a low surface area of 5 $m^2 g^{-1}$ (Figure S8a). However, the **HFGO@ZIF-8** hybrid shows both type-I (micropores originating from the surface of the ZIF-8) and type-IV isotherms (mesopores due

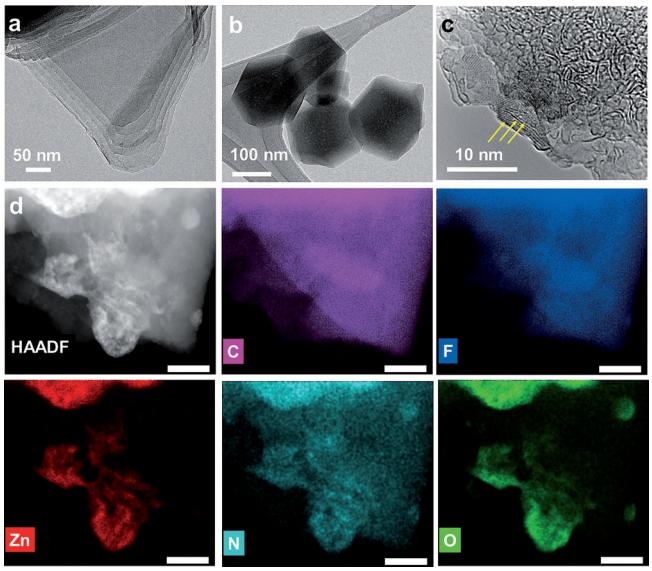

Figure 2. TEM images of a) HFGO and b) ZIF-8 nanocrystals c) HRTEM image of the **HFGO@ZIF-8** composite; ZIF-8 nanocrystals intercalated between HFGO multilayers indicated by arrows. d) HAADF-STEM image and EDS chemical mapping of the **HFGO@-ZIF-8** composite showing the spatial distribution of the elements C, F, Zn, N, and O. Scale bars correspond to 70 nm.

to the stacking of ZIF-8 nanocrystals between HFGO layers) with a sharp capillary condensation step in the relative pressure range of 0.5–0.7. The BET surface area of the composite was found to be quite high with 590 $m^2 g^{-1}$ (Figure 3). The pore size distribution calculated by using the nonlocal density functional theory (NLDFT) method gives a binodal pore size distribution. Pore sizes of 1 nm are assigned to ZIF-8 and the 3 nm range is assigned to mesopores in the composite structure (see Figure S8 and Figure 3 inset).

The various characterization techniques indicate the homogeneous dispersion of ZIF-8 nanocrystals between HFGO layers. Young's equation suggests that the surface

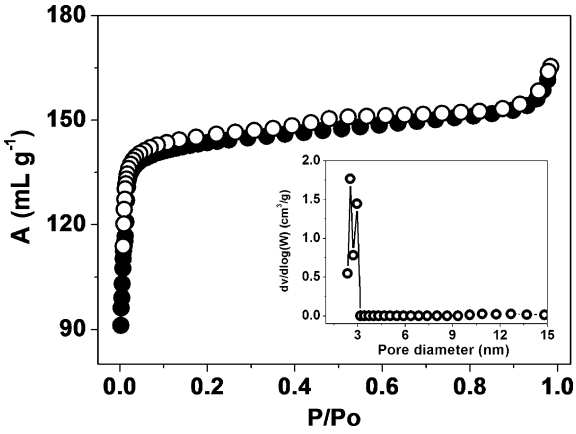

Figure 3. Nitrogen adsorption (black circles), desorption (white circles) isotherm of the **HFGO@ZIF-8** composite; inset shows the pore size distribution.

energy of the solid surface is a key factor for its hydrophobicity. Contact angle measurements were performed to investigate the wettability of the **HFGO@ZIF-8** composite. A pellet of pristine ZIF-8 showed a water contact angle of about 56° (Figure 4a). HFGO showed a water contact angle of 125° (hydrophobic nature) due to the high proportion of covalent C–F bonds (Figure 4b). For the **HFGO@ZIF-8** composite the water droplet assumes a remarkably large contact angle of 162°, indicating the superhydrophobic behavior of the composite (Figure 4c); this value ranks **HFGO@ZIF-8** among the top five known materials for oil–water separation (Table S1).[6] Indeed, water droplets deposited on the **HFGO@ZIF-8** surface were observed to form almost perfect spheres (Figure S9a,b). Videos demonstrating the superhydrophobic behavior of the **HFGO@ZIF-8** composite are available in the Supporting Information and the time-dependent contact angle measurements confirm constant super-hydrophobicity (Figure S10, ca. 3 min). Interestingly, an oil droplet rapidly penetrates into the composite in less than 15 s, and the oil contact angle was measured to be 0° suggesting the superoleophilic nature (Figure 4d and Figure S11).

The self-cleaning ability of a **HFGO@ZIF-8** pellet was demonstrated by placing it in a volume of 1 L water followed by the addition of silicone oil (Figure S12a–c). The composite material **HFGO@ZIF-8** (activated at 160 °C) was further exploited for the absorption of oils and various organic solvents. The relative absorption capacity of the samples was calculated using the following equation: $(W_{wet}-W_{intial})/W_{intial}\times 100\,\%$, where $W_{initial}$ and W_{wet} are the weights of initial and wet samples, respectively.

ZIF-8 itself shows an absorption capacity in the range of 10–150 wt %, while HFGO shows negligible uptake. In contrast the absorption capacity of **HFGO@ZIF-8** is much enhanced and ranges between 20 and 280 wt %. These values are superior to those reported for resins and other porous composites.[16] The absorption capacity of the composite is much better than that of the two individual pristine components due to the micro-mesopore structure along with the effective dispersion of the nanoparticles between HFGO layers; this distribution is controlled by the distribution of oxygen-atom-containing surface nucleation centers for ZIF-8 growth. The powder XRD image confirms that the structural properties of the **HFGO@ZIF-8** composite are fully retained after absorbing these polar and nonpolar organic solvents (SI, Figure S13), highlighting the robust nature of the composite assembly.

Based on these results, we fabricated **Sponge@HFGO@-ZIF-8** by immersing a commercial sponge into the reaction mixture of exfoliated HFGO and a methanolic solution of the ZIF-8 growth components and letting it sit in solution overnight (see the Experimental Section in the Supporting Information). The choice of a sponge as the support material is due to its macroporous nature and its absorption of both water and oil. **Sponge@HFGO@ZIF-8** shows excellent absorption capacities for nonpolar and polar organic solvents and oils achieving 150–600 wt % depending on the oil or solvent (Figure 4f). Furthermore the sponge floats on water and the extraction of oil or organic solvent can be easily

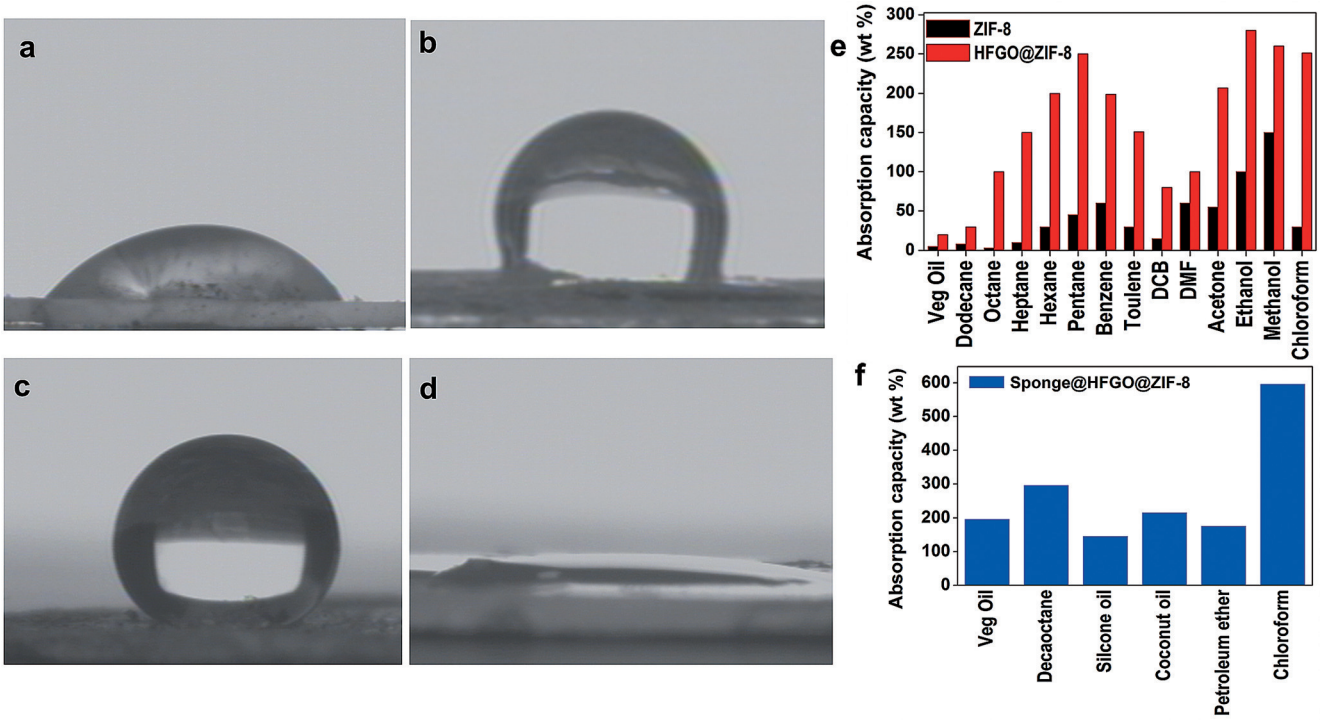

Figure 4. Photographs demonstrating the hydrophobicity of ZIF-8 with a water contact angle of 56° (a) and HFGO with a water contact angle of 125° (b), and the superhydrophobicity of the **HFGO@ZIF-8** hybrid showing water contact angle of 162° (c) and an oil contact angle of 0° (d). e) Absorption of oil and organic solvents with ZIF-8 and the **HFGO@ZIF-8** composite (DCB:dichlorobenzene) and f) oil absorption with **Sponge@HFGO@ZIF-8**.

achieved (Figure S12d). This demonstrates a perspective for practical applications of **HFGO@ZIF-8** and related materials.

In summary, a simple and scalable method is reported for the fabrication of a superhydrophobic and at the same time superoleophilic and as well hierarchical micro-mesoporous hybrid material based on ZIF-8 nanocrystals intercalated between highly fluorinated graphene oxide sheets. Among the existing materials for oil–water separation, this is the first in which fluorographene serves as a functional scaffold for immobilizing MOF nanoparticles (Table S1). The synergistic properties of the surface energy of C–F groups, the alkyl-substituted imidazole groups, nanoscale roughness, and micro-mesoporous nanoarchitecture yield a composite material for the selective absorption of polar and nonpolar organic solvents from water with excellent absorption capacities. The materials design concept is based on the selective nucleation and controlled growth of ZIF-8 nanocrystals due to Zn^{II} chelation with the surface oxygen functionalities of the HFGO structure. Our results suggest an avenue for the preparation of novel multifunctional composites of 2D graphene materials and nanocrystalline MOFs, with an application potential not only in water purification but also for advanced solar cells, biosensors, photocatalysts, and magnetic and electronic devices.

Acknowledgements

This work was supported by the "Cluster of Excellence RESOLV" funded by the Deutsche Forschungsgemeinschaft (EXC 1069; C.R., graduate fellowship). K.J.R. is grateful to the Alexander von Humboldt foundation. K.K.R.D., M.P., M.O., and R.Z. acknowledge support by Palacký University, and the Ministry of Education, Youth and Sports of the Czech Republic (LO1305), and by Technology Agency "Competence Centers" (TE01020218). M.P. is grateful for an internal student grant (Palacký University, IGA_PrF_2015_017). We thank Ondrej Tomanec for HRTEM analysis.

Keywords: highly fluorinated graphene oxide · oil–water separation · superhydrophobicity · superoleophilicity · zeolite imidazole frameworks

How to cite: *Angew. Chem. Int. Ed.* **2016**, *55*, 1178–1182
Angew. Chem. **2016**, *128*, 1193–1197

[1] a) M. H. Jin, J. Wang, X. Yao, M. Y. Liao, Y. Zhao, L. Jiang, *Adv. Mater.* **2011**, *23*, 2861–2864; b) Z. Chu, Y. Feng, S. Seeger, *Angew. Chem. Int. Ed.* **2014**, *53*, 2711–2715; *Angew. Chem.* **2014**, *126*, 2749–2753.
[2] K. Gaaseidnes, J. Turbeville, *Pure Appl. Chem.* **1999**, *71*, 95–101.
[3] T. Darmanin, F. Guittard, *J. Mater. Chem. A* **2014**, *2*, 16319–16359.
[4] Y. L. Song, B. Q. Liu, L. Jiang, D. B. Zhu, *Adv. Mater.* **2002**, *14*, 1857–1860.

[5] N. García, E. Benito, J. Guzman, P. Tiemblo, *J. Am. Chem. Soc.* **2007**, *129*, 5052 – 5060.
[6] B. Wang, W. Liang, Z. Guo, W. Liu, *Chem. Soc. Rev.* **2015**, *44*, 336 – 361.
[7] X. J. Feng, L. Jiang, *Adv. Mater.* **2006**, *18*, 3063 – 3078.
[8] W. X. Liang, Z. G. Guo, *RSC Adv.* **2013**, *3*, 16469 – 16474.
[9] a) S. Kitagawa, *Angew. Chem. Int. Ed.* **2015**, *54*, 10686 – 10687; b) V. Stavila, A. A. Talin, M. D. Allendorf, *Chem. Soc. Rev.* **2014**, *43*, 5994 – 6010; c) Z. Fang, B. Bueken, D. E. De Vos, R. A. Fischer, *Angew. Chem. Int. Ed.* **2015**, *54*, 7234 – 7254; *Angew. Chem.* **2015**, *127*, 7340 – 7362; d) A. K. Cheetham, C. N. R. Rao, *Science* **2007**, *318*, 58 – 59; e) W. Xia, A. Mahmood, R. Zou, Q. Xu, *Energy Environ. Sci.* **2015**, *8*, 1837 – 1866.
[10] a) K. P. Rao, M. Higuchi, K. Sumida, S. Furukawa, J. Duan, S. Kitagawa, *Angew. Chem. Int. Ed.* **2014**, *53*, 8225 – 8230; *Angew. Chem.* **2014**, *126*, 8364 – 8369; b) H. J. Jeon, R. Matsuda, P. Kanoo, H. Kajiro, L. Li, H. Sato, Y. Zheng, S. Kitagawa, *Chem. Commun.* **2014**, *50*, 10861 – 10863; c) T. H. Chen, I. Popov, O. Zenasni, O. Daugulis, O. S. Miljanic, *Chem. Commun.* **2013**, *49*, 6846; d) C. Yang, U. Kaipa, Q. Z. Mather, X. Wang, V. Nesterov, A. F. Venero, M. A. Omary, *J. Am. Chem. Soc.* **2011**, *133*, 18094; e) A. Fernandez, S. K. Nune, H. V. Annapureddy, L. X. Dang, B. P. McGrail, F. Zheng, E. Polikarpov, D. L. King, C. Freeman, K. P. Brooks, *Dalton Trans.* **2015**, *44*, 13490 – 13497.
[11] a) C. Petit, T. J. Bandosz, *Adv. Mater.* **2009**, *21*, 4753 – 4757; b) R. Kumar, K. Jayaramulu, T. K. Maji, C. N. R. Rao, *Chem. Commun.* **2013**, *49*, 4947 – 4949; c) M. Jahan, Q. Bao, J.-X. Yang, K. P. Loh, *J. Am. Chem. Soc.* **2010**, *132*, 14487 – 14495; d) H.-x. Zhong, J. Wang, Y.-w. Zhang, W.-l. Xu, W. Xing, D. Xu, Y.-f. Zhang, X.-b. Zhang, *Angew. Chem. Int. Ed.* **2014**, *53*, 14235 – 14239; *Angew. Chem.* **2014**, *126*, 14459 – 14463.
[12] a) R. Zboril, F. Karlicky, A. B. Bourlinos, T. A. Steriotis, A. K. Stubos, V. Georgakilas, K. Safarova, D. Jancik, C. Trapalis, M. Otyepka, *Small* **2010**, *6*, 2885; b) "Halogenated Graphenes: Emerging Family of Two-Dimensional Materials": K. K. R. Datta, R. Zboril in *Functionalization of Graphene* (Ed.: V. Georgakilas), Wiley-VCH, Weinheim, **2014**, pp. 173 – 198; c) F. Karlický, K. K. R. Datta, M. Otyepka, R. Zboril, *ACS Nano* **2013**, *7*, 6434 – 6464.
[13] a) K. S. Park, Z. Ni, A. P. Côté, J. Y. Choi, R. Huang, F. J. Uribe-Romo, H. K. Chae, M. O'Keeffe, O. M. Yaghi, *Proc. Natl. Acad. Sci. USA* **2006**, *103*, 10186 – 10191; b) B. Chen, Z. Yang, Y. Zhu, Y. Xia, *J. Mater. Chem. A* **2014**, *2*, 16811 – 16831.
[14] a) M. Tu, S. Wannapaiboon, K. Khaletskaya, R. A. Fischer, *Adv. Funct. Mater.* **2015**, *25*, 4470 – 4479; b) M. Tu, S. Wannapaiboon, R. A. Fischer, *Inorg. Chem. Front.* **2014**, *1*, 442 – 463; c) O. Shekhah, M. Eddaoudi, *Chem. Commun.* **2013**, *49*, 10079 – 10081.
[15] M. Eddaoudi, D. F. Sava, J. F. Eubank, K. Adil, V. Guillerm, *Chem. Soc. Rev.* **2015**, *44*, 228 – 249.
[16] G. R. Shan, P. Y. Xu, Z. X. Weng, Z. M. Huang, *J. Appl. Polym. Sci.* **2003**, *89*, 3309 – 3314.

Received: August 17, 2015
Published online: December 7, 2015

